Zigzag phase transition in the frustrated Ising honeycomb lattice

P. F. Dias and M. Schmidt ⓘ[*]

Departamento de Física, Universidade Federal de Santa Maria, 97105-900 Santa Maria, Rio Grande do Sul, Brazil

We investigate the thermal phase transitions of the J_1-J_2-J_3 Ising model on the honeycomb lattice. This model exhibits the zigzag (ZZ) antiferromagnetic phase, which is observed in the Ising honeycomb compound FePS$_3$. By employing a cluster mean-field approach, we describe the role of exchange couplings on phase transitions and thermodynamics of the model. We found first- and second-order transitions between ZZ and paramagnetic phases. Moreover, the model hosts thermal order-by-disorder state selection and, for weak third-neighbor couplings, signatures of strong frustration, such as a round maximum in the specific heat. Our results provide a picture for the nature of thermally driven phase transitions in a wide range of exchange interactions. We show that the first-order phase transition observed in FePS$_3$ is hosted by the present microscopic model by adopting exchange couplings from literature.

I. INTRODUCTION

The inability to simultaneously satisfy all interactions in frustrated spin systems introduce a conflicting situation that can strongly affect the stability of magnetic phases, altering the criticality and the thermodynamics at low temperatures. In these systems, dimensionality plays a significant role on critical phenomena, with low-dimensional magnets seemingly more sensitive to frustration effects [1]. Within the Ising model, well-known examples of frustrated two-dimensional (2D) systems include the antiferromagnetic triangular [2] and J_1-J_2 square lattices [3]. In the former, conventional long-range order is absent at finite temperatures and thermodynamic signatures of strong frustration arise, including residual entropy [2,4] and a round maximum in the specific heat [5]. In the latter, phase boundaries can exhibit continuous and discontinuous order-disorder phase transitions, including tricriticality, depending on the ratio between first- and second-neighbor interactions [6].

From the experimental point of view, numerous efforts have been made to produce and characterize 2D magnets, which is often motivated by the rich phenomenology and potential applications of these materials [7]. Recently, research on van der Waals materials provided significant advances in the field, including the experimental realization of atomically thin magnets [8]. Within this class of materials, several transition metal phosphorus trisulfide compounds, such as FePS$_3$ [9], MnPS$_3$ [10], and NiPS$_3$ [11], emerged as promising candidates for technological application of 2D magnets [8,12]. In addition, these compounds host antiferromagnetic long-range order within the honeycomb lattice structure formed by the transition metal magnetic ions, providing platforms for the study of magnetic phase transitions at the monolayer limit [13].

Among the transition metal phosphorus trisulfide compounds, FePS$_3$ provides a unique example of a 2D magnet with Ising anisotropy [9]. Iron atoms in bulk FePS$_3$ form weakly-interacting layers of a graphenelike structure that orders into a zigzag (ZZ) antiferromagnetic phase (see Fig. 1) below the Néel temperature $T_N \approx 120$ K [14–17]. Attempts to model the unusual antiferromagnetic structure observed in FePS$_3$ showed that exchange interactions up to third-neighbors in a honeycomb lattice should be taken into account [16,18,19]. These results also indicate that frustrated exchange interactions are hosted by FePS$_3$, making it prototypical to investigate the role of competing interactions in 2D magnetism. In addition, mechanical exfoliation allows obtaining atomically thin layers that exhibit analogous magnetic properties of bulk FePS$_3$, with T_N remaining almost independent of thickness [9]. It is also worth noting that early studies of bulk FePS$_3$ proposed that the transition between ZZ and paramagnetic (PM) phases is a first-order phase transition [14,20,21]. This hypothesis has been corroborated by spin wave measurements of a powdered sample of FePS$_3$ [18] and is also in agreement with the magnetic specific heat sharp peak [22] and a steep variation in magnetic susceptibility observed near T_N [9,14]. Despite the vast relevance of the compound, the origin of the first-order ZZ-PM phase transition observed in FePS$_3$ remains elusive.

In the present work, we investigate the thermal phase transitions of an Ising model with interactions between first (J_1), second (J_2), and third neighbors (J_3) on the honeycomb lattice. We focus in the case with ferromagnetic (FE) J_1 and antiferromagnetic J_3, which allows obtaining the ZZ phase hosted by FePS$_3$ at low temperatures [16,18,19]. In order to investigate the phase transitions of the model, we employ the cluster mean-field (CMF) method with clusters of up to 18 sites [23–28]. This framework provides an estimate for the system free energy, allowing the stability analysis of phases, the identification of the nature of phase transitions and the derivation of thermodynamic quantities. It is worth noting that

[*]mateus.schmidt@ufsm.br

this method has been widely applied in the study of phase transitions in frustrated magnets, such as the Ising [29] and Heisenberg [30,31] models on the triangular lattice and the Ising [32] and Heisenberg [33] models on the J_1-J_2 square lattice. In particular, the CMF accuracy to identify the coupling coordinate of the tricritical point in the frustrated Ising model on the square lattice matches the state-of-the-art Monte Carlo simulations [30]. In a recent work, the CMF method was employed to investigate the J_1-J_2 Ising model on the honeycomb lattice, incorporating thermodynamic signatures of strong frustration introduced by competing interactions [34]. Therefore, the method allows incorporating frustration effects in phase diagrams and thermodynamics, which is of utmost importance for the present study.

The rest of the paper is organized as follows. In Sec. II, the model is described and the ground-state energy of the relevant phases is calculated. The CMF implementation for this particular model is also described in detail. Our results, including phase diagrams and thermodynamic quantities, are presented in Sec. III. The conclusion of the paper is given in Sec. IV.

II. MODEL AND METHOD

We considered a honeycomb lattice with Ising spins at the vertices and exchange couplings between pairs of first, second, and third neighbors. The Hamiltonian of this system is given by

$$H = -\sum_{i,j} J_{ij}\sigma_i\sigma_j - h\sum_i \sigma_i, \tag{1}$$

where J_{ij} is equal to J_1, J_2, or J_3, h is the external magnetic field, and $\sigma_i = \pm 1$ is the Ising spin variable of site i. This model exhibits a rich ground-state phase diagram with several types of antiferromagnetic phases. In a recent study [16], mean-field calculations for the model with FE first-neighbor couplings indicated that four types of antiferromagnetism can compete with the FE ground state in the absence of external field. It is found that FE third-neighbor interactions and antiferromagnetic J_2 can lead to an armchair (for weak J_3) or a stripe (for strong J_3) phase. When antiferromagnetic third-neighbor couplings are considered, the onset of the ZZ phase or the Néel antiferromagnet (for strong J_3 and a ferromagnetic J_2) can be observed. Although the ground state of the model has been thoroughly described, the effects of temperature (T) on the phase diagrams remains an open problem. In particular, the exact solution for this model is known only for the limit case $J_2 = J_3 = 0$, exhibiting a ferromagnetic long-range order that breaks a twofold symmetry below the reduced critical temperature $k_B T_c/J_1 \approx 1.52$ (k_B is the Boltzmann constant) [35,36].

In the present work, we focus on the case in the absence of external magnetic field ($h = 0$) with ferromagnetic first-neighbor interactions ($J_1 > 0$) and antiferromagnetic couplings between third neighbors, i.e., $-1 < J_3/J_1 < 0$, a scenario in which the ZZ antiferromagnetic phase can be found. In Fig. 1, we present the six ZZ ground states, in which the third-neighbor interactions are fully satisfied, but J_1 and J_2 are only partially satisfied. The ground-state energy per site of this phase is given by $U_{ZZ}(T = 0) = (3J_3 + 2J_2 - J_1)/2$.
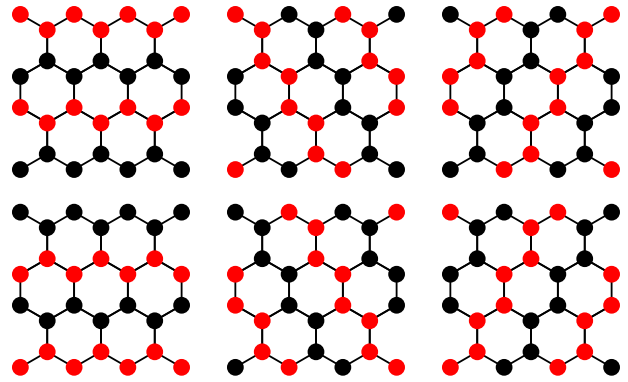

FIG. 1. The six zigzag microscopic ground states. The states described in the lower panels can be obtained by global spin inversion of the states described in the upper panels.

By comparing this energy with the one for the ferromagnetic phase $U_{FE}(T = 0) = (-3J_3 - 6J_2 - 3J_1)/2$, one can build the ground-state phase diagram of the model within the range of parameters considered in the present work.

In order to investigate the thermal phase transitions hosted by this model, we employ a cluster mean-field approximation in Eq. (1). In this method, the system is divided into N_{cl} identical clusters of size n_s. The interactions between magnetic moments that belong to the same cluster are incorporated exactly, while the couplings between spins from different clusters are approximated using the usual mean-field approach

$$\sigma_i\sigma_j \approx \sigma_i\langle\sigma_j\rangle + \langle\sigma_i\rangle\sigma_j - \langle\sigma_i\rangle\langle\sigma_j\rangle, \tag{2}$$

where $\langle\sigma_i\rangle$ is the local magnetization (m_i) of site i. The method accuracy is only bounded by the ability to compute the partition function of large cluster systems, that should account for the 2^{n_s} spin states. In the present work, we adopt clusters of $n_s = 1$, 6, and 18, as shown in Fig. 2. In the following, we discuss each case.

A. Mean-field approach

First, let us consider a single-site approximation, which is equivalent to the standard mean-field theory and, therefore, no intracluster interaction is taken into account. In the FE phase, local magnetizations are identical, i.e., $m_i = m_j$. On the other hand, in order to employ the mean-field approach to the ZZ phase, one must consider the sublattices within this long-range order. Figure 2(a) illustrates the mean fields acting on a single site, with red and black sites belonging to sublattices A and B, respectively. Here, we assume that the local magnetization from sites belonging to different sublattices can be related in the form $m_i^A = -m_j^B$, where m_i^A (m_j^B) belongs to the sublattice A (B).

Taking into account the magnetization pattern of each phase, the local magnetizations can be evaluated from the self-consistent equation

$$m = \langle\sigma\rangle = \tanh{(\beta m \lambda_{FE/ZZ})}, \tag{3}$$

where $\beta = 1/k_B T$. For the ferromagnetic phase $\lambda_{FE} = 3J_1 + 6J_2 + 3J_3$, and for the ZZ phase $\lambda_{ZZ} = J_1 - 2J_2 - 3J_3$. It is worth noting that m is the magnetization per site for the
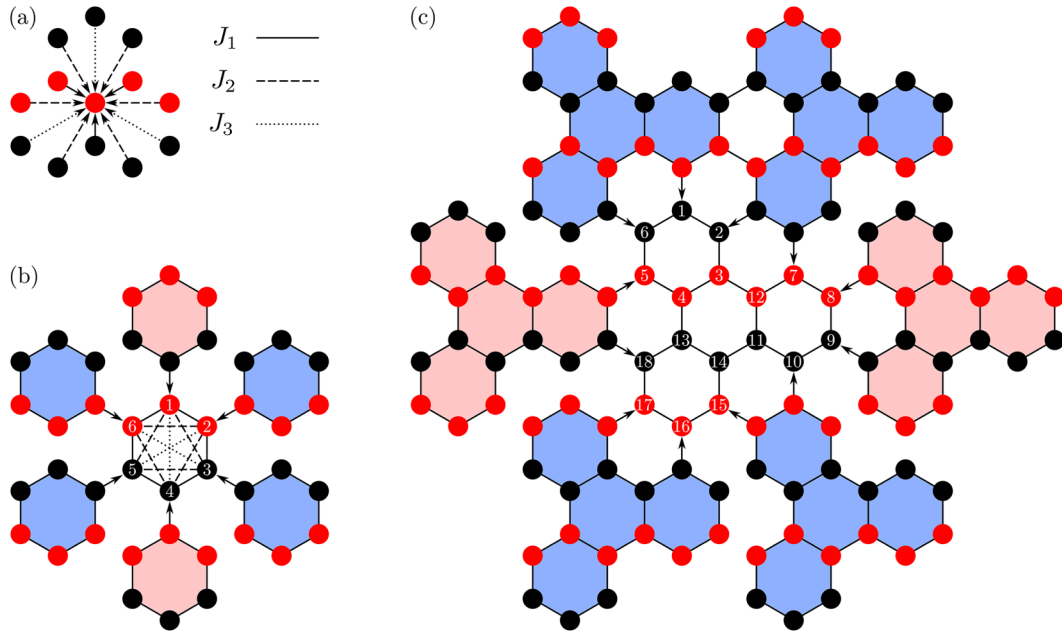
FIG. 2. The clusters adopted in the cluster mean-field approach with the colors in filled circles (representing magnetic sites) following the zigzag pattern. Solid, dashed, and dotted lines represent first-, second-, and third-neighbor interactions, respectively. (a) The single-site (standard mean field) approximation with mean fields represented by arrows. (b) The six-site cluster approach, with first-neighbor mean-fields and all intracluster interactions in the central cluster. Panel (c) shows the 18-site cluster with mean fields and intracluster interactions related only to first-neighbor interactions. Red clusters exhibit the same local magnetization pattern of the central cluster, while blue clusters show a local magnetization pattern with opposite sign of the equivalent sites from the central cluster.

FE phase and the staggered magnetization for the ZZ phase. After solving the self-consistent problem of Eq. (3), thermodynamic quantities can be evaluated from the free-energy per spin

$$f = -k_B T \ln \left[\cosh \left(\beta \, m \, \lambda_{FE/ZZ} \right) \right] + \lambda_{FE/ZZ} \, m^2 / 2. \quad (4)$$

The free energy is also useful to locate first-order phase transitions, which is done by comparing its value for each of the phases in the transformation.

B. Cluster mean-field approach

The single-site mean-field theory provides a simple framework to investigate phase transitions. However, by neglecting correlations, the method is unable to incorporate some important effects of frustration. A straightforward improvement of the standard mean-field treatment can be achieved by employing clusters of spins instead of canonical spins. In other words, this framework allows to incorporate exactly the interactions within the clusters. More important, frustration effects introduced by intracluster interactions are incorporated exactly. The cluster mean-field method has been employed to the study of the honeycomb lattice in recent investigations [34,37]. In particular, in Ref. [34], the frustrated J_1-J_2 Ising model was investigated by employing the CMF method with the six-site cluster of Fig. 2(b) and the 18-site cluster shown in Fig. 2(c). It is worth noting that this particular choice of cluster shapes allows obtaining the sixfold degeneracy of the ZZ phase.

By employing the approximation of Eq. (2) in the intercluster couplings, the many-body problem is reduced to a

single-cluster Hamiltonian given by

$$H_{CMF} = -\sum_{\langle i,j \rangle} J_{ij} S_i S_j - \sum_{i,j} J_{ij} \left[S_i m'_j - \frac{m_i m'_j}{2} \right], \quad (5)$$

where m_i is a local magnetization from a site within the central cluster and m'_j are mean-fields from neighbor clusters. In the ferromagnetic phase, one can relate the local magnetization from the neighbor cluster to equivalent sites from the central cluster (i.e., $m'_j = m_j$). However, for the ZZ phase, this straightforward relation is not always valid. In particular, clusters highlighted in blue exhibit a magnetization pattern that differs from the central one [see panels (b) and (c) of Fig. 2]. It means that the cluster boundary conditions must be adapted to the local magnetization pattern of the ZZ phase, as done in a recent CMF study of a spin-1 model with competing interactions [38]. In fact, sites from blue clusters show a local magnetization with the same absolute value (but opposite sign) of the topologically equivalent sites from the central cluster. It means that the relation $m'_j = -m_j$ is valid when considering blue clusters, and $m'_j = m_j$ for red clusters.

These relations between local magnetizations of the central cluster and its neighbors allow to obtain an effective single-cluster problem amenable to a self-consistent solution. In principle, one can compute all local magnetizations, but a reduced number of independent self-consistent parameters can be obtained, depending on the cluster size and the long-range order.

Let us now focus on the $n_s = 6$ cluster, in which all sites are topologically equivalent. We can write this Hamiltonian in

the form

$$H_{\text{CMF-6}} = H_6' + H_{\text{MF-6}}, \qquad (6)$$

where

$$
\begin{aligned}
H_6' = & -J_1[\sigma_1(\sigma_2 + \sigma_6) + \sigma_3(\sigma_2 + \sigma_4) + \sigma_5(\sigma_4 + \sigma_6)] \\
& -J_2[\sigma_1(\sigma_5 + \sigma_3) + \sigma_2(\sigma_4 + \sigma_6) + \sigma_3\sigma_5 + \sigma_4\sigma_6] \\
& -J_3[\sigma_1\sigma_4 + \sigma_2\sigma_5 + \sigma_3\sigma_6]
\end{aligned}
$$

incorporates the intracluster couplings and $H_{\text{MF-6}}$ is the mean-field contribution. In the ferromagnetic phase, all sites exhibit the same local magnetization. It means that the CMF problem is reduced to a single self-consistent parameter. For instance, we can write the mean-field contribution as a function of m_1:

$$H_{\text{MF-6}}^{FE} = -(J_1 + 4J_2 + 2J_3)\left(m_1 \sum_{i=1}^{6} \sigma_i - 3m_1^2\right). \qquad (7)$$

In the ZZ phase, the six-site cluster mean-field approximation introduces an inhomogeneity within the sublattices. For instance, site 1 is not equivalent to sites 2 and 6. It is worth stressing that this inhomogeneity is an artifact of the CMF method instead of a feature of the model. Thus, there are two independent self-consistent parameters. We can reduce the effective problem to the computation of the local magnetizations from sites 1 and 2. Noting that $m_1 = -m_4$ and $m_2 = m_6 = -m_3 = -m_5$, the mean-field contribution is given by

$$
\begin{aligned}
H_{\text{MF-6}}^{ZZ} = & (\sigma_1 - \sigma_4 - m_1)(J_1 m_1 + 2J_3 m_2) \\
& + (\sigma_3 - \sigma_2 + \sigma_5 - \sigma_6 + 2m_2)(-J_3 m_1 \\
& + [J_1 - 2J_2 - J_3]m_2).
\end{aligned} \qquad (8)
$$

After solving the self-consistent problem, the free energy per spin

$$f_{\text{CMF-6}} = -\frac{\ln\left(\text{Tr}\, e^{-\beta H_{\text{CMF-6}}}\right)}{n_s \beta} \qquad (9)$$

can be evaluated. In addition, entropy per spin $S = (U - f_{\text{CMF-6}})/T$ and specific heat $C_v = dU/dT$ can be computed by using the internal energy per spin

$$U = \langle H_{\text{CMF-6}} \rangle = \frac{\text{Tr}\, H_{\text{CMF-6}}\, e^{-\beta H_{\text{CMF-6}}}}{n_s\, \text{Tr}\, e^{-\beta H_{\text{CMF-6}}}}. \qquad (10)$$

The order parameter of each phase can be computed from the local magnetizations. The magnetization per site $m_{FE} = \sum_{i=1}^{n_s} m_i/n_s$ is the order parameter of the ferromagnetic phase while the staggered magnetization

$$m_{ZZ} = (m_1 + m_2 + m_6 - m_3 - m_4 - m_5)/n_s \qquad (11)$$

is the order parameter of the zigzag phase.

The implementation of the CMF method for the 18-site cluster shown in Fig. 2(c) follows in an analogous way. However, for this larger cluster, there are more independent mean-field parameters, which leads to lengthy equations that will be discussed in the Appendix. For instance, the ZZ phase leads to nine independent mean-field parameters for $n_s = 18$. In order to classify the nature of phase transitions, we compare the free energy of different phases. For the order-disorder
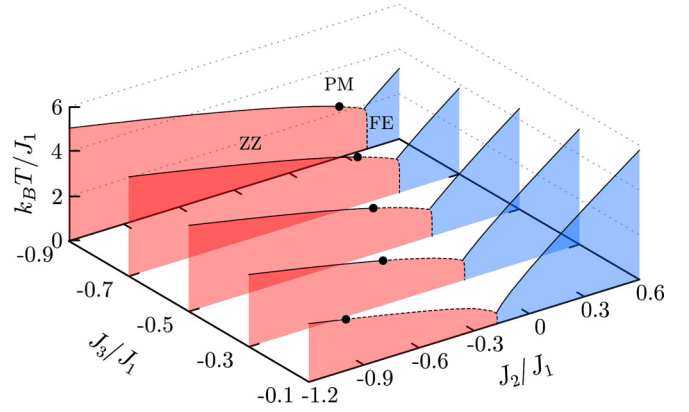

FIG. 3. Phase diagram of temperature *versus* second-neighbor couplings for several strengths of J_3/J_1. Continuous and dashed lines indicate second-order and first-order phase transitions, respectively. Filled circles indicate the tricritical points.

phase transitions, we compare the free energies as a function of temperature adopting a reduced temperature step of 10^{-5}. We classified the transition as first order when the free energies of the phases showed a crossing point. Second-order phase transitions were characterized by the absence of a crossing point.

III. RESULTS

In this section, we present the numerical results obtained from the mean-field and cluster mean-field treatment of the J_1-J_2-J_3 Ising model on the honeycomb lattice. In order to compare our findings with the magnetic behavior of FePS$_3$, we consider a ferromagnetic J_1 interaction, which is used as unit of energy. In addition, we focus on antiferromagnetic third-neighbor couplings, assuming that these interactions are finite and weaker than the first-neighbor couplings. In the following, we report our findings allowing ferromagnetic and antiferromagnetic second-neighbor couplings.

In Fig. 3, we present the global phase diagram of the model obtained within the six-site CMF approximation. The temperature-coupling phase diagrams show FE and ZZ ground states with a boundary between these two phases located in agreement with the ground-state energies. When thermal fluctuations are considered, frustration effects can be noted in the phase diagram. In particular, for $J_3/J_1 = -0.1$, a ferromagnetic second-neighbor coupling leads to the onset of a ferromagnetic phase below a Curie temperature T_C. We also note that only second-order phase transitions are observed in the FE-PM phase boundary. Moreover, reducing J_2 brings down T_C until the ZZ phase takes place for $J_2 \leqslant -0.175J_1$. A first-order phase transition separates the long-range orders at low temperatures.

In the ZZ-PM phase boundary, a very interesting scenario arises with the onset of first-order order-disorder phase transitions. Moreover, for strong antiferromagnetic interactions between second neighbors, second-order ZZ-PM phase transitions can be found, with a tricritical point indicating the change in the nature of phase transitions. In Fig. 4, we present the behavior of thermodynamic quantities within the six-site CMF calculation. For $J_3/J_1 = -0.1$, a discontinuity
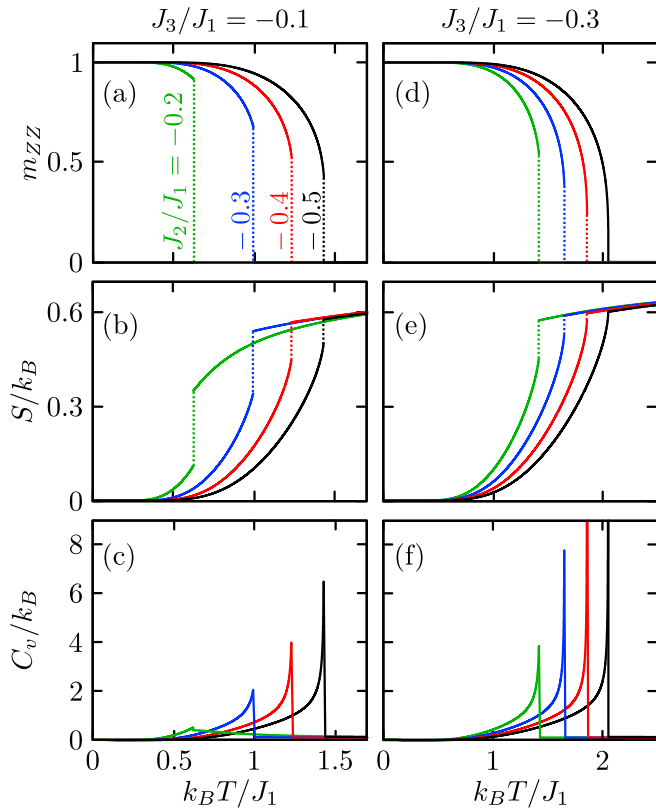
FIG. 4. Thermodynamics within the six-site CMF approximation. The order parameter, entropy per spin, and specific heat as functions of temperature are exhibited for $J_3/J_1 = -0.1$ (left column) and $J_3/J_1 = -0.3$ (right column) and several strengths of second-neighbor couplings. A dotted line indicates the discontinuity in the order parameter and entropy.

can be observed in the ZZ phase order parameter and in the entropy per spin as functions of temperature for $J_2/J_1 = -0.2, -0.3, -0.4$, and -0.5. These discontinuities are signatures of the ZZ-PM first-order phase transitions that take place for these strengths of second-neighbor couplings. The specific heat also exhibits a discontinuity at the transition, but the behavior of this quantity cannot be used to unambiguously identify the nature of phase transitions. Moreover, increasing the strength of second-neighbor interactions enhance the ZZ-PM ordering temperature. We also note that the jump in the entropy and order parameter is reduced while approaching the tricritical point, which takes place at $J_2/J_1 \approx -1.0$ for $J_3/J_1 = -0.1$. An even more interesting scenario can be observed in Fig. 4 for $J_3/J_1 = -0.3$. In this case, thermodynamic signatures of first-order phase transitions are observed for $J_2/J_1 = -0.2, -0.3$, and -0.4. On the other hand, for $J_2/J_1 = -0.5$, the order parameter and entropy show a continuous behavior at the phase transition, indicating a second-order phase transition. This qualitative change in the thermodynamic behavior of the system signals a change in the nature of the phase transitions, indicating the presence of a tricritical point between $J_2/J_1 = -0.4$ and $J_2/J_1 = -0.5$. We also note that the specific heat becomes sharper at the transition as the tricritical point is approached.
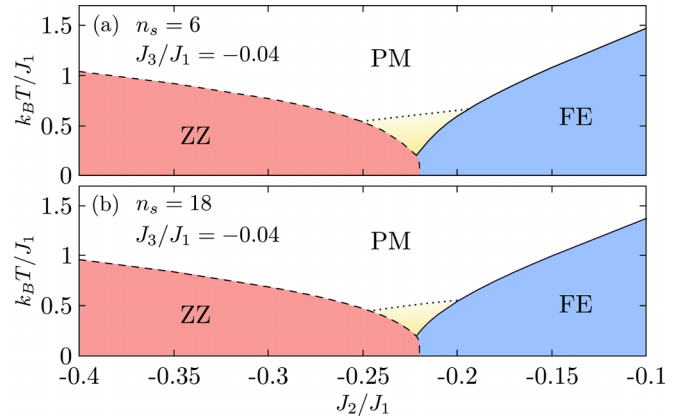

FIG. 5. Phase diagrams in the temperature-coupling plane for $J_3/J_1 = -0.04$ adopting (a) $n_s = 6$ and (b) $n_s = 18$. The same convention of Fig. 3 is adopted. The dotted line indicates a crossover within the paramagnetic phase located at the specific heat maximum.

Our data supports that tricriticality takes place for all strengths of J_3/J_1 considered for both $n_s = 6$ and $n_s = 18$ clusters. We also note that stronger antiferromagnetic third-neighbor couplings enhance the Néel temperature, and therefore favors the ZZ phase. This result is expected once a negative J_3 coupling favors anti-aligned third neighbors, driving a ZZ phase that is more robust under thermal fluctuations. Then, one can expect that stronger frustration effects take place when this interaction is weaker.

In Fig. 5, we present the coupling-temperature phase diagram for weak third-neighbor couplings ($J_3/J_1 = -0.04$) obtained within the CMF method with clusters of size $n_s = 6$ and $n_s = 18$. The single-site mean-field results show continuous order-disorder phase transitions and are omitted. The ground-state transition between the two ordered phases takes place at $J_2/J_1 = -0.22$, in agreement with the exact ground-state energies presented in Sec. II. As a consequence of the strong competition between these two ordered states, the order-disorder transition reaches its lowest values for $J_2/J_1 \approx -0.22$. In addition, we found a second maximum of specific heat in the PM phase, which can be related to the onset of a correlated paramagnetic phase. The dotted line indicates the temperature in which this second maximum occurs. It is worth noting that the J_1-J_2 Ising model on the honeycomb lattice also exhibits a maximum of specific heat above the ordering temperature [34]. Therefore this round maximum of specific heat can be understood as a remnant effect of the strongly frustrated scenario found when $J_3 = 0$.

In order to further reason about the frustration effects, we present results for the thermodynamics of the model at very weak third-neighbor couplings in Fig. 6 ($J_3/J_1 = -0.04$). We note that for $J_2/J_1 = -0.3$, entropy exhibits a discontinuity and specific heat shows a sharp peak at the ZZ-PM phase transition, which is expected for a first-order phase transition. For $J_2/J_1 = -0.222$, cooling down the system from high temperatures leads to a significant entropy drop, which is followed by a specific heat maximum. At even lower temperatures, entropy and specific heat show a discontinuity at the ZZ-PM phase transition. For temperatures above the FE-PM phase transition, similar phenomena can be noted in the specific heat and
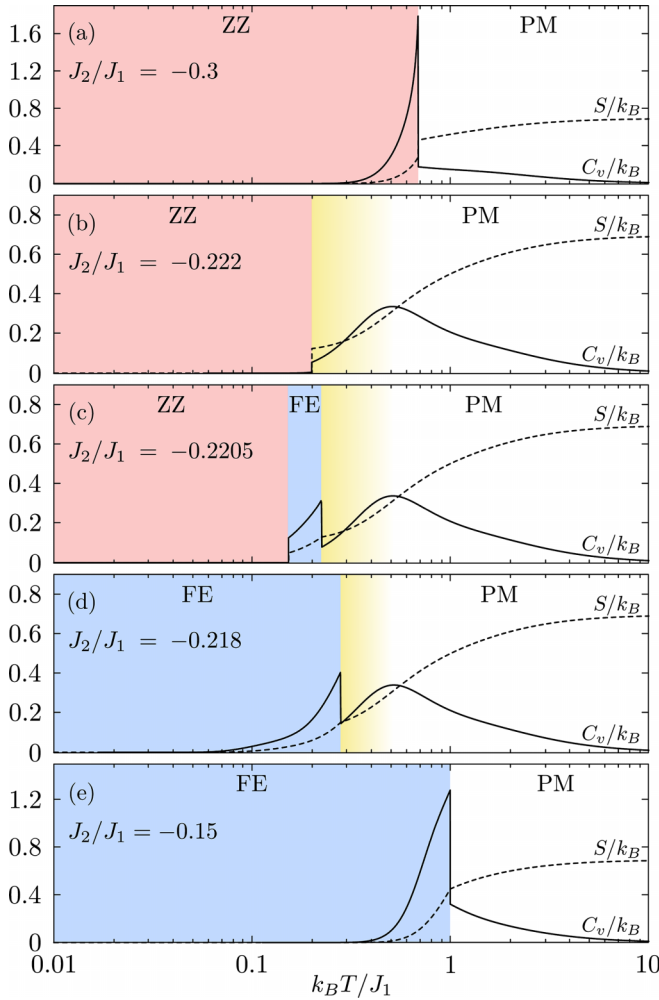
FIG. 6. Thermal dependence of specific heat and entropy per spin for $J_3/J_1 = -0.04$ and several strengths of second-neighbor interactions within the 18-site CMF approximation. Colors delimit the range of temperature in which each phase is found.

FIG. 7. Difference between free energies per spin of FE and ZZ phases ($\Delta f = f_{FE} - f_{ZZ}$) as a function of temperature for coupling strengths that correspond to the ground-state level crossing between these phases. Panel (a) exhibits the data for $n_s = 6$ and 18 at $J_3/J_1 = -0.04$ and $J_2/J_1 = -0.22$. In panel (b), results for $n_s = 6$ when $J_3/J_1 = -0.1$ ($J_2/J_1 = -0.175$), $J_3/J_1 = -0.3$ ($J_2/J_1 = -0.025$), and $J_3/J_1 = -0.5$ ($J_2/J_1 = 0.125$) are shown.

energy. Therefore, thermal fluctuations select the FE phase at low temperatures. In Fig. 7(a), our data for $J_3/J_1 = -0.04$ and $J_2/J_1 = -0.22$ show that this phenomenon can be observed for $n_s = 6$ and $n_s = 18$. In addition, the order-by-disorder state selection takes place at different coupling strengths, as shown in Fig. 7(b). Analogous phenomenon was reported in recent CMF [39] as well as Monte Carlo and Bethe lattice [40] studies of the frustrated Ising bilayer honeycomb lattice.

The FePS$_3$ compound shows signatures of a first-order phase transition between ZZ and PM phases. Therefore, it is interesting to consider whether the present model can incorporate the nature of the ZZ-PM phase transition hosted by FePS$_3$. As shown in Fig. 3, first-order phase transitions can be found at different strengths of J_3/J_1 and J_2/J_1. In Ref. [19], the magnon dynamics of FePS$_3$ was investigated by means of neutron inelastic scattering. A good fit to the experimental results was achieved by adopting $J_1 = 1.46$ meV, $J_2 = -0.04$ meV, and $J_3 = -0.96$ meV within a Heisenberg model. In order to investigate whether this set of couplings allows us to obtain the appropriate nature of phase transitions in the present model, we adopt the exchange couplings considered in Ref. [19]. In Fig. 8, we present the phase diagrams for clusters of $n_s = 1$, 6, and 18 by considering $J_3/J_1 = -0.66$. We note that the range in which first-order phase transitions

entropy [see, e.g., panel (d) of Fig. 6]. We also note that the entropy is continuous at the FE-PM phase transition, which is expected for second-order phase transitions. We remark that the signatures of frustration spotted in the present model are restricted to the neighborhood of the FE-ZZ ground-state level crossing. In particular, for $J_2/J_1 = -0.15$, the maximum in the specific heat within the PM phase is absent as shown in Fig. 6(e).

Our results also indicate an order-by-disorder thermal selection of the FE phase. This reentrant phenomenon can be spotted in Fig. 6(c), where heating up the zigzag antiferromagnet leads the system into the ferromagnetic phase for $J_2/J_1 = -0.2205$. The order-by-disorder state selection can also be observed in the behavior of free energy. In Fig. 7, we present the difference of the free energy per site between ZZ and FE phases as a function of temperature. The coupling strengths are set to correspond to the ground-state ZZ-FE phase transition. It means that at absolute zero temperature, the free energy of both phases is the same. As temperature is increased, a finite difference between the free energies of these phases can be noted, with the FE phase showing a lower free
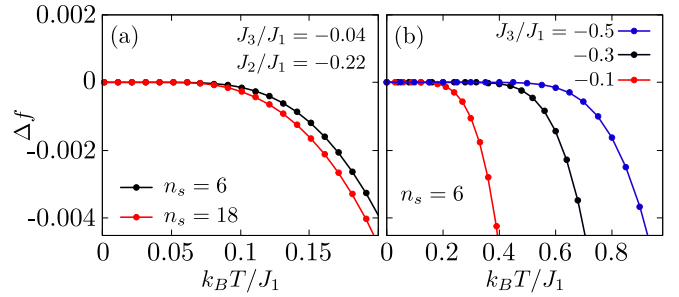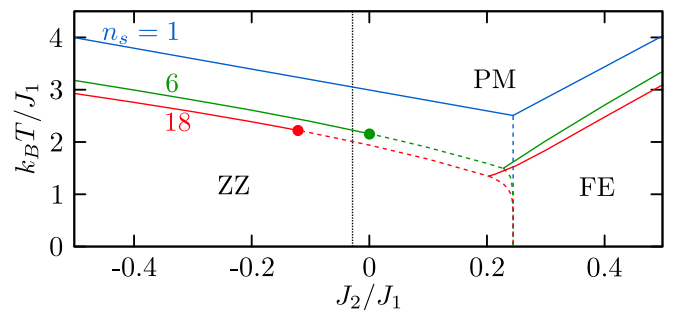

FIG. 8. Phase diagram of temperature *versus* coupling for $J_3/J_1 = -0.66$ within the single-site mean-field and CMF approximations. The same convention of Fig. 3 is adopted. The vertical dotted line is placed at $J_2/J_1 = -0.027$, corresponding to the exchange estimate from Ref. [19].
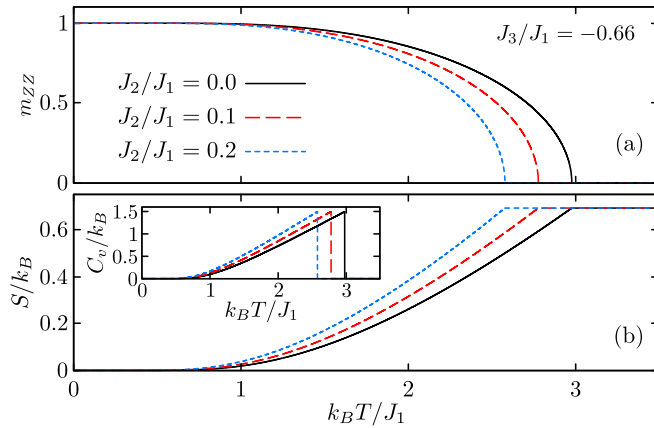
FIG. 9. Thermal dependence of the (a) zigzag phase order parameter and (b) entropy per spin for $J_3/J_1 = -0.66$ and several strengths of J_2/J_1 within the single-site CMF approximation. The inset in panel (b) shows the specific heat as a function of temperature.
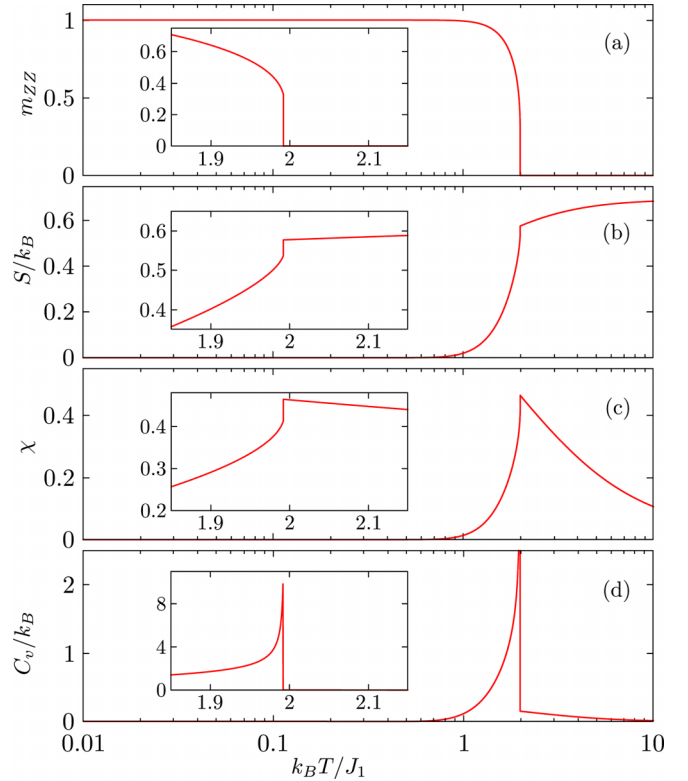

FIG. 10. Thermal dependence of the (a) zigzag phase order parameter, (b) entropy per spin, (c) magnetic susceptibility, and (d) specific heat for $J_2/J_1 = -0.027$ and $J_3/J_1 = -0.66$ within 18-site CMF approximation. The insets show the quantities near the phase transition.

are obtained depends on the level of the CMF approximation. For instance, the single-site mean-field treatment suggests that only second-order ZZ-PM phase transitions can be observed. In Fig. 9, we present the mean-field results for the thermodynamics of the model for $J_3/J_1 = -0.66$ and several strengths of second-neighbor couplings. While the ZZ order parameter and entropy exhibit a continuous behavior, the specific heat shows a discontinuity at the phase transition, which is consistent with second-order phase transitions. However, the CMF results for $n_s = 6$ and $n_s = 18$ suggests the existence of first-order phase transitions and tricriticality at the ZZ-PM phase boundary. We note that the six-site CMF approximation delivers a tricritical point at $J_2/J_1 \approx 0.00$, indicating that a second-order phase transition takes place for the experimentally relevant strength of second-neighbor couplings $J_2/J_1 = -0.027$. However, the 18-site approach indicates a first-order ZZ-PM phase transition for the same strength of J_2/J_1 (see the dotted line in Fig. 8), with a tricritical point at $J_2/J_1 \approx -0.12$. Considering that larger clusters provide better results within the CMF approach, our findings indicate that the phase transition arising when $J_3/J_1 = -0.66$ and $J_2/J_1 = -0.027$ is a first-order phase transition. Therefore, our results indicate that the exchange couplings proposed in Ref. [19] allows us to correctly reproduce the nature of the ZZ-PM phase transition observed in FePS$_3$.

Experimental results indicate that the magnetic specific heat of FePS$_3$ exhibits a sharp peak at the ZZ-PM phase transition, which can be attributed to the discontinuous nature of the phase transition. In Fig. 10, we present the behavior of the order parameter m_{ZZ}, magnetic susceptibility, specific heat and entropy per spin as functions of temperature for exchange parameters in agreement with Ref. [19] ($J_3/J_1 = -0.66$ and $J_2/J_1 = -0.027$). Entropy and the order parameter exhibit a discontinuity at the phase transition, as expected for first-order phase transitions. We also note that the magnetic susceptibility lacks the round maximum above the ordering temperature observed in bulk FePS$_3$. On the other hand, $\chi(T)$ exhibits the abrupt drop near the phase transition reported in Ref. [9]. Moreover, the inset of Fig. 10(c) exhibits the discontinuous behavior of the magnetic susceptibility at the ordering

temperature, in agreement with the experimental results. More interesting, the specific heat exhibits a sharp peak at T_N, as evidenced by the inset in Fig. 10(d). Therefore, our microscopic model calculations allows to qualitatively reproduce the behavior of specific heat observed for FePS$_3$ by adopting the exchange couplings proposed in Ref. [19].

It is worth noting that similar behavior of thermodynamic quantities can be obtained in the range of parameters in which first-order phase transitions are present. In order to have a more clear picture for the range of parameters in which first-order ZZ-PM phase transitions can be found in the present model, we gathered data from our CMF calculations in Fig. 11. We remark that fits to experimental results suggest that $J_2 \approx 0$ and $|J_3|$ should be weaker but comparable with J_1 [16,19]. Therefore, we focus our analysis on $J_3/J_1 \leqslant -0.3$. Our findings suggest that lowering J_3/J_1 from -0.3 down to -0.9 reduces the range of J_2/J_1 in which first-order ZZ-PM phase transitions can be found. Moreover, assuming a weak second-neighbor coupling narrows the range of J_3/J_1 in which first-order phase transitions take place. For instance, constraining the absolute value of J_2 so that $|J_2|/J_1 < 0.05$ allows first-order phase transitions in a range of third-neighbor couplings that is roughly between $J_3/J_1 \approx -0.3$ and -0.8 according to our 18-site CMF results. It is also worth noting that the filled square in Fig. 11 corresponds to the estimate of exchange couplings for FePS$_3$ from Ref. [19], which is seemingly close to the tricritical point.
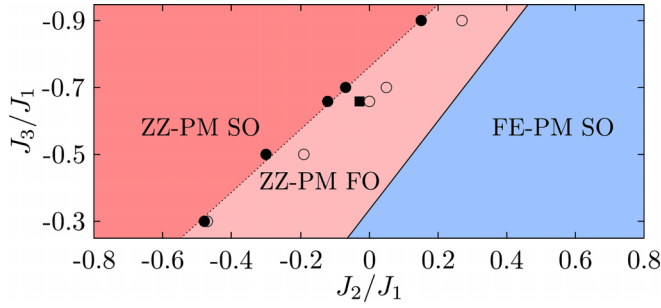
FIG. 11. Coupling coordinates of the tricritical points computed within the CMF approximation for $n_s = 6$ (empty circles) and $n_s = 18$ (filled circles). The solid line indicates the ground-state ZZ-FE phase transition. The dashed line is a guide for the eyes following the trend for the tricritical points obtained within the 18-site approximation. This trend allows to visualize regions in which first-order (FO) and second-order (SO) phase transitions arise at the ZZ-PM thermal phase transition. The filled square corresponds to the exchange estimate for FePS$_3$ proposed in Ref. [19].

IV. CONCLUSION

We investigated the thermal phase transitions and thermodynamics of the J_1-J_2-J_3 Ising model on the honeycomb lattice. Phase diagrams were obtained for ferromagnetic first-neighbor interactions and antiferromagnetic third-neighbor couplings ($-1 < J_3/J_1 < 0$) within a cluster mean-field approach with clusters of up to 18 sites. Our findings indicate that the ZZ-PM phase boundary can exhibit several interesting phenomena, including the onset of first-order phase transitions and tricriticality. For weak third-neighbor couplings, strong frustration effects take place close to the boundary between ordered phases. In particular, a round maximum is found in the thermal dependence of the specific heat, a thermodynamic behavior that is often observed in strongly frustrated systems such as the Ising triangular [5] and kagome lattices [41,42].

We also focus on the range of exchange couplings that are relevant to the zigzag phase transition found in FePS$_3$. In particular, our CMF calculations provide an estimate for the range of exchange parameters in which the model exhibits first-order phase transitions. We note that the exchange couplings estimated for FePS$_3$ in Ref. [19], namely $J_2/J_1 = -0.027$ and $J_3/J_1 = -0.66$, allows us to obtain a first-order ZZ-PM phase transition for $n_s = 18$. Therefore, our results indicate that the J_1-J_2-J_3 Ising model on the honeycomb lattice can be a minimal model to obtain not only the type of unusual magnetism observed in FePS$_3$, but also is able to correctly incorporate the nature of the phase transition observed in this 2D magnet. We expect that the rich phenomenology unveiled within the CMF approach motivates studies of the present model within other analytical and numerical methods. An interesting question concerns the critical exponents of the ZZ-PM phase transition, which can be investigated within Monte Carlo simulations.

It is worth remarking that our microscopic model calculations do not cover the vast complexity of FePS$_3$ and further investigations are required to draw a complete picture for the magnetism of this compound. For instance, we neglect any spin interacting term beyond the Ising coupling

and the possibility of different strengths of interactions between equivalent neighbors [43]. We also note that although very weak, interlayer interactions in bulk FePS$_3$ might be relevant for the nature of phase transitions. We believe that incorporating some of these features in the present model can lead to challenging and exciting problems. In fact, it has been shown that pressure can reduce the interlayer distance, driving a stronger coupling between crystal planes of FePS$_3$ [17]. We note that recent results for the J_1-J_2 Ising model on the square lattice indicate that the nature of phase transitions can be strongly affected by interlayer couplings [44]. Therefore, an interesting question for future research concerns whether interlayer exchange interactions can affect the nature of phase transitions exhibited by the J_1-J_2-J_3 Ising model on the honeycomb lattice. Moreover, the role of external magnetic fields in the present model is also a subject worth investigating. The possibility of a field-induced tricritical point was hinted in an investigation of the high field magnetization of FePS$_3$ [16]. Our findings suggest that the present model is prone to exhibit a tricritical point, which might be also obtained by incorporating effects of transverse and longitudinal external fields. In our opinion, the CMF method is a feasible approximation to carry out these studies.

APPENDIX: CMF THEORY FOR THE 18-SITE CLUSTER

In this Appendix, we describe the CMF implementation for the cluster of size $n_s = 18$ shown in Fig. 2(c). By adopting the mean-field approximation of Eq. (2) in the intercluster interactions, we can reduce the many-body problem to a single-cluster effective problem with Hamiltonian

$$H_{\text{CMF-18}} = H'_{18} + H_{\text{MF}-18}. \tag{A1}$$

The intracluster term can be written in the form

$$H'_{18} = H'_1 + H'_2 + H'_3, \tag{A2}$$

where

$$\begin{aligned} H'_1 = -J_1[&\sigma_1(\sigma_2 + \sigma_6) + \sigma_5(\sigma_4 + \sigma_6) + \sigma_7(\sigma_8 + \sigma_{12}) \\ &+ \sigma_3(\sigma_2 + \sigma_4 + \sigma_{12}) + \sigma_{11}(\sigma_{10} + \sigma_{12} + \sigma_{14}) \\ &+ \sigma_9(\sigma_8 + \sigma_{10}) + \sigma_{13}(\sigma_4 + \sigma_{14} + \sigma_{18}) \\ &+ \sigma_{15}(\sigma_{14} + \sigma_{16}) + \sigma_{17}(\sigma_{16} + \sigma_{18})], \end{aligned}$$

$$\begin{aligned} H'_2 = -J_2[&\sigma_1(\sigma_3 + \sigma_5) + \sigma_3(\sigma_5 + \sigma_7 + \sigma_{11} + \sigma_{13}) \\ &+ \sigma_2(\sigma_4 + \sigma_6 + \sigma_{12}) + \sigma_{12}(\sigma_8 + \sigma_{10} + \sigma_{14}) \\ &+ \sigma_7(\sigma_9 + \sigma_{11}) + \sigma_4(\sigma_6 + \sigma_{12} + \sigma_{14} + \sigma_{18}) \\ &+ \sigma_{11}(\sigma_9 + \sigma_{13} + \sigma_{15}) + \sigma_{14}(\sigma_{16} + \sigma_{18}) \\ &+ \sigma_{13}(\sigma_5 + \sigma_{15} + \sigma_{17}) + \sigma_{10}(\sigma_8 + \sigma_{14}) \\ &+ \sigma_{15}\sigma_{17} + \sigma_{16}\sigma_{18}], \end{aligned}$$

and

$$
\begin{aligned}
H_3' = & -J_3[\sigma_2(\sigma_5 + \sigma_7) + \sigma_3(\sigma_6 + \sigma_{14}) + \sigma_4(\sigma_1 + \sigma_{11}) \\
& + \sigma_8\sigma_{11} + \sigma_{10}(\sigma_7 + \sigma_{15}) + \sigma_{12}(\sigma_9 + \sigma_{13}) \\
& + \sigma_{18}(\sigma_5 + \sigma_{15}) + \sigma_{13}\sigma_{16} + \sigma_{14}\sigma_{17}].
\end{aligned}
$$

The mean-field term can be written in a compact form by considering the local magnetization pattern of the phases under consideration. In the following, we discuss this term for the FE and ZZ phases.

1. The ferromagnetic solution

The intercluster term within the CMF implementation must account for different local magnetizations within the cluster. This difference is an artifact of the method and only takes place due to sites that are topologically inequivalent within the cluster and/or sublattice. For the FE phase, the local magnetizations of the central hexagon in 18-site cluster are identical, i.e., $m_3 = m_4 = m_{11} = m_{12} = m_{13} = m_{14}$. The outermost sites of the cluster can exhibit two different local magnetizations. The sites that are linked by the first-neighbor intracluster couplings to the central hexagon exhibit the same magnetization, which means that $m_2 = m_5 = m_7 = m_{10} = m_{15} = m_{18}$. Finally, the remaining sites are also topologically equivalent, allowing to write $m_1 = m_6 = m_8 = m_9 = m_{16} = m_{17}$.

In the FE case, the local magnetization pattern of all clusters is the same, which means that the local magnetization

from neighbor clusters can be obtained from equivalent sites of the central cluster. Thus, the intercluster term can be written as

$$
\begin{aligned}
H_{\text{MF-18}}^{\text{FE}} = & -J_1[S_2 m_1 + S_1 m_2 - 6m_1 m_2] \\
& -J_2\big[S_1(2m_1 + m_3 + m_2) + S_2(2m_2 + m_1) \\
& + S_3 m_1 - 6\big(m_1^2 + m_1 m_3 + m_1 m_2 + m_2^2\big)\big] \\
& -J_3[S_1(m_3 + m_2) + (S_2 + S_3)m_1 \\
& - 6m_1(m_2 + m_3)],
\end{aligned}
$$

where $S_1 = \sigma_1 + \sigma_6 + \sigma_8 + \sigma_9 + \sigma_{16} + \sigma_{17}$, $S_2 = \sigma_2 + \sigma_5 + \sigma_7 + \sigma_{10} + \sigma_{15} + \sigma_{18}$ e $S_3 = \sigma_3 + \sigma_4 + \sigma_{11} + \sigma_{12} + \sigma_{13} + \sigma_{14}$.

2. The zigzag solution

In the ZZ phase, we can identify two types of clusters within the 18-site approximation. The red clusters in Fig. 2(c) exhibit the same local magnetization pattern of the central cluster. On the other hand, the blue clusters in Fig. 2(c) exhibit local magnetizations (m_i') with opposite sign of the local magnetizations from equivalent sites of the central cluster (m_i). It means that $m_i' = -m_i$.

In addition, within the central cluster, the local magnetizations respect the relations $m_1 = -m_{16}$, $m_2 = -m_{15}$, $m_3 = -m_{14}$, $m_4 = -m_{13}$, $m_5 = -m_{18}$, $m_6 = -m_{17}$, $m_7 = -m_{10}$, $m_8 = -m_9$, and $m_{12} = -m_{11}$. Using these relations, we can write the intercluster term of the CMF Hamiltonian as

$$
\begin{aligned}
H_{\text{MF-18}}^{\text{ZZ}} = & -J_1[\mu_1 m_7 + \mu_2 m_2 + \mu_3 m_1 + \mu_4 m_5 + \mu_5 m_6 + \mu_6 m_8 - 2(m_1 m_7 + m_5 m_8 + m_6 m_2)] - J_2[m_3\mu_2 + m_4\mu_4 \\
& + m_1(\mu_5 + \mu_2 + \mu_4 + \mu_7) + m_2(\mu_1 + \mu_6 + \mu_3) + m_5(\mu_5 + \mu_3 - \mu_4) + m_6(\mu_1 + \mu_8 + \mu_3 + \mu_4) + m_{12}\mu_1 \\
& + m_7(\mu_5 + \mu_6 + \mu_2) + m_8(\mu_1 + \mu_9 - \mu_6 + \mu_2) + 2\{m_5(m_8 - m_7) - m_1(m_8 + m_2 + m_{12} + m_6) \\
& - m_2(m_5 + m_7) - m_6(m_3 + m_7) - m_8(m_4 + m_6)\}] - J_3[(\mu_8 + \mu_6)m_1 + \mu_4(m_2 - m_4) + \mu_1(m_3 + m5) \\
& + (\mu_3 + \mu_7)m_6 + \mu_2(m_7 + m_{12}) + (\mu_5 - \mu_9)m_8 - 2m_1(m_3 + m_5) - 2m_8(m_2 - m_4) - 2m_6(m_7 + m_{12})],
\end{aligned}
$$

where $\mu_1 = \sigma_1 - \sigma_{16}$, $\mu_2 = \sigma_6 - \sigma_{17}$, $\mu_3 = \sigma_7 - \sigma_{10}$, $\mu_4 = \sigma_8 - \sigma_9$, $\mu_5 = \sigma_2 - \sigma_{15}$, $\mu_6 = \sigma_5 - \sigma_{18}$, $\mu_7 = \sigma_{12} - \sigma_{11}$, $\mu_8 = \sigma_3 - \sigma_{14}$, and $\mu_9 = \sigma_4 - \sigma_{13}$.

In order to investigate the magnetic susceptibility $\chi = dm/dh$ within the ZZ phase, we employ a numerical derivative of the magnetization. It means that the magnetization in the presence of a small external field should be evaluated. At a finite external field, the local magnetizations of different sublattices do not hold a straightforward

relation. As a consequence, the 18 local magnetizations should be evaluated. The local magnetizations from the blue clusters can be obtained from sites within the central cluster that holds an equivalent position within the sublattice. For instance, the magnetization m_1 is equivalent to the magnetization m_{16}' from the blue clusters. Analogous relations can be established for all local magnetizations of the blue clusters, allowing us to obtain the self-consistent equations.

[1] B. Schmidt and P. Thalmeier, Phys. Rep. **703**, 1 (2017).

[2] G. H. Wannier, Phys. Rev. **79**, 357 (1950).

[3] M. Nauenberg and B. Nienhuis, Phys. Rev. Lett. **33**, 944 (1974).

[4] G. H. Wannier, Phys. Rev. B **7**, 5017 (1973).

[5] M. Rigol, T. Bryant, and R. R. P. Singh, Phys. Rev. E **75**, 061118 (2007).

[6] S. Jin, A. Sen, and A. W. Sandvik, Phys. Rev. Lett. **108**, 045702 (2012).

[7] B. Huang, M. A. McGuire, A. F. May, D. Xiao, P. Jarillo-Herrero, and X. Xu, Nat. Mater. **19**, 1276 (2020).

[8] Q. H. Wang, A. Bedoya-Pinto, M. Blei, A. H. Dismukes, A. Hamo, S. Jenkins, M. Koperski, Y. Liu, Q.-C. Sun, E. J. Telford, H. H. Kim, M. Augustin, U. Vool, J.-X. Yin, L. H. Li, A. Falin,

C. R. Dean, F. Casanova, R. F. L. Evans, M. Chshiev *et al.*, ACS Nano **16**, 6960 (2022).

[9] J.-U. Lee, S. Lee, J. H. Ryoo, S. Kang, T. Y. Kim, P. Kim, C.-H. Park, J.-G. Park, and H. Cheong, Nano Lett. **16**, 7433 (2016).

[10] G. Long, H. Henck, M. Gibertini, D. Dumcenco, Z. Wang, T. Taniguchi, K. Watanabe, E. Giannini, and A. F. Morpurgo, Nano Lett. **20**, 2452 (2020).

[11] X. Wang, J. Cao, H. Li, Z. Lu, A. Cohen, A. Haldar, H. Kitadai, Q. Tan, K. S. Burch, D. Smirnov, W. Xu, S. Sharifzadeh, L. Liang, and X. Ling, Sci. Adv. **8**, eabl7707 (2022).

[12] J.-G. Park, J. Phys.: Condens. Matter **28**, 301001 (2016).

[13] M. Šiškins, M. Lee, S. Mañas-Valero, E. Coronado, Y. M. Blanter, H. S. van der Zant, and P. G. Steeneken, Nat. Commun. **11**, 2698 (2020).

[14] P. Jernberg, S. Bjarman, and R. Wäppling, J. Magn. Magn. Mater. **46**, 178 (1984).

[15] P. A. Joy and S. Vasudevan, Phys. Rev. B **46**, 5425 (1992).

[16] A. R. Wildes, D. Lançon, M. K. Chan, F. Weickert, N. Harrison, V. Simonet, M. E. Zhitomirsky, M. V. Gvozdikova, T. Ziman, and H. M. Rønnow, Phys. Rev. B **101**, 024415 (2020).

[17] M. J. Coak, D. M. Jarvis, H. Hamidov, A. R. Wildes, J. A. M. Paddison, C. Liu, C. R. S. Haines, N. T. Dang, S. E. Kichanov, B. N. Savenko, S. Lee, M. Kratochvílová, S. Klotz, T. C. Hansen, D. P. Kozlenko, J.-G. Park, and S. S. Saxena, Phys. Rev. X **11**, 011024 (2021).

[18] A. R. Wildes, K. C. Rule, R. I. Bewley, M. Enderle, and T. J. Hicks, J. Phys.: Condens. Matter **24**, 416004 (2012).

[19] D. Lançon, H. C. Walker, E. Ressouche, B. Ouladdiaf, K. C. Rule, G. J. McIntyre, T. J. Hicks, H. M. Rønnow, and A. R. Wildes, Phys. Rev. B **94**, 214407 (2016).

[20] S. Bjarman, P. Jernberg, and R. Wäppling, Hyperfine Interact. **16**, 625 (1983).

[21] P. Ferloni and M. Scagliotti, Thermochim. Acta **139**, 197 (1989).

[22] Y. Takano, N. Arai, A. Arai, Y. Takahashi, K. Takase, and K. Sekizawa, J. Magn. Magn. Mater. **272-276**, E593 (2004).

[23] D. Yamamoto, G. Marmorini, and I. Danshita, Phys. Rev. Lett. **112**, 127203 (2014).

[24] D. Yamamoto, G. Marmorini, and I. Danshita, Phys. Rev. Lett. **114**, 027201 (2015).

[25] A. Singhania and S. Kumar, Phys. Rev. B **98**, 104429 (2018).

[26] N. Kellermann, M. Schmidt, and F. M. Zimmer, Phys. Rev. E **99**, 012134 (2019).

[27] A. Singhania and S. Kumar, Phys. Rev. B **101**, 064403 (2020).

[28] M. Schmidt, G. Kohlrausch, and F. Zimmer, Physica A **596**, 127126 (2022).

[29] T. Yokota, Phys. Rev. E **89**, 012128 (2014).

[30] D. Yamamoto, G. Marmorini, M. Tabata, K. Sakakura, and I. Danshita, Phys. Rev. B **100**, 140410(R) (2019).

[31] D. Yamamoto, C. Suzuki, G. Marmorini, S. Okazaki, and N. Furukawa, Phys. Rev. Lett. **125**, 057204 (2020).

[32] S. Jin, A. Sen, W. Guo, and A. W. Sandvik, Phys. Rev. B **87**, 144406 (2013).

[33] Y.-Z. Ren, N.-H. Tong, and X.-C. Xie, J. Phys.: Condens. Matter **26**, 115601 (2014).

[34] M. Schmidt and P. Godoy, J. Magn. Magn. Mater. **537**, 168151 (2021).

[35] R. Houtappel, Physica **16**, 425 (1950).

[36] J. Strečka and M. Jaščur, Acta Physica Slovaca **65**, 235 (2015).

[37] A. F. Albuquerque, D. Schwandt, B. Hetényi, S. Capponi, M. Mambrini, and A. M. Läuchli, Phys. Rev. B **84**, 024406 (2011).

[38] G. L. K. Frantz, M. Schmidt, and F. M. Zimmer, Phys. Rev. E **103**, 032125 (2021).

[39] L. C. Rossato, F. Zimmer, C. Morais, and M. Schmidt, Physica A **621**, 128778 (2023).

[40] F. A. Gómez Albarracín, H. D. Rosales, and P. Serra, Phys. Rev. E **98**, 012139 (2018).

[41] M. Semjan and M. Žukovič, Phys. Lett. A **384**, 126615 (2020).

[42] M. Schmidt, F. M. Zimmer, and S. G. Magalhaes, J. Phys.: Condens. Matter **29**, 165801 (2017).

[43] A. R. Wildes, M. E. Zhitomirsky, T. Ziman, D. Lançon, and H. C. Walker, J. Appl. Phys. **127**, 223903 (2020).

[44] P. F. Godoy, M. Schmidt, and F. M. Zimmer, Phys. Lett. A **384**, 126687 (2020).